CHAPTER –V

CHAPTER - V

5 X-RAY K-ABSORPTION SPECTRAL STUDIES OF COPPER COMPLEXES USING SYNCHROTRON RADIATION SOURCES

5.1 Introduction

X-ray absorption fine structure (XAFS) spectroscopy becomes a powerful technique providing analytical as well as structural information, with applications in a wide range of scientific fields because of the rapid development of the data treatment techniques. Synchrotron X-ray absorption fine structure spectroscopy is an effective technique for selectively investigating the local coordination environment of metal ions.

It is important and interesting to understand the physico-chemical properties of copper complexes with newly synthesized Schiff bases which are of biological interest. Schiff[143] was the first to carry out the condensation of primary amines with the compounds containing carbonyl group. Therefore, the condensation products are often referred to as Schiff bases. They are also called imines or azomethines. By means of various studies, it has been shown that C=N- group has significant biological importance[144]. In C=N- group, nitrogen is trigonally hybridized and there is a possibility of having a lone pair of electron in either a π or a sp^2 hybridized orbital. This is of fundamental chemical and biological importance. The various angles of hybridization make the formation of nitrogen containing molecules possible which with the associated delicate differences in their physico- chemical properties produce the necessary various phenomena of life.

The number of drugs is metal binding agents. Schiff bases possess analgesic, anti-inflammatory, antibiotic, antiulcer, and anti- microbial activities. Schiff bases exhibit anticancer activity. They have been found to be effective against Mycobacterium tuberculosis. Due to the diverse applications of the Schiff bases, their

[143] Schiff H, Ann. 1864 Chem. 131, 118().
[144] Kumar S., D.N. Dhar and P.N. Saxena, J. Sci. Ind. Res. 68, 181 (2009).

metal complexes have been synthesized. Transition metal ions plays vital role in a vast number of biological processes and ions with biologically active ligands are subject of considerable interest. The samples of Schiff base ligand have been prepared because they have great biological importance, and have found application as antifungal, antibacterial, antitumor, polymers, antifertility and dyes etc. Previous reports have shown that they have good enhanced activities due to their complex formation.

Schiff bases have been playing an important part in the development of Co-ordination chemistry. Schiff base metal complexes have been studied extensively because of their attractive chemical and physical properties and their wide range of applications in numerous scientific areas. They play an important role in both synthetic and structural research, because of their preparative accessibility and structural diversity1. Schiff bases of o-phenylenediamine and its complexes have a variety of applications including biological, clinical and analytical. Schiff's bases derived from aromatic amines and aromatic aldehydes and its complexes have a wide variety of applications in many fields, e.g., biological, inorganic and analytical chemistry[145]. Schiff bases of o-phenylenediamine and its complexes have a variety of applications including biological, analytical and clinical. Metal complexes of Schiff base are extensively studied due to synthetic flexibility and sensitivity toward a variety of metal atoms. They are found useful in catalysis, in medicine as antibiotics and anti-inflammatory agent and in the industry as anti-corrosion[146]. It has been found that all the complexes are antimicrobially active and show higher activity than the free ligand.

In the present chapter, we have carried out study of X-ray K-absorption spectra of series of Ten copper(II)complexes viz. Bis-pentanyl R(sbstituted anilene)-phenyldiazine Cu(II) bis-benzenediamine in ortho(2) para(3) and meta(4) positioned, the complex is already pointed out in chapter II. The XAFS spectra were recorded at recently developed DEXAFS beamline BL-8 at the Indus-2 synchrotron source at RRCAT, Indore. The complexes are given in table 5.1.

[145] Ramana. N., L.Mitub, A. Sakthivela , M.S.S. Pandia , *J. Iran.Chem. Soc.*, **6(4)** ,738, (2009).
Theis B., S. Metz, F. Back, C. Burschka, R. Tacke, *Z anorg. allg. Chem.*, **635,** 1306 (2009).
[146] Dhar D N & Taploo C L, Schiff bases and their applications, *J Sci Ind Res*, **41** ,1982, **501-506**

Table 5.1 Copper (II) complexes, abbreviation and molecular formula.			
S.No	**Complex name**	**Abbreviation**	**Molecular formula**
1.	Bis-pentanyl R(4-Nitro)-phenyldiazine Cu(II) bis-benzenediamine	Bisp(4-Nitro) pdCu(II)bisbd	**$C_{32}H_{26}N_{10}O_4Cl_2Cu$**
2.	Bis-pentanyl R(pure anilene)- phenyldiazine Cu(II) bis-benzenediamine	Bisp(pureanilene)pdCu(II) bisbd	**$C_{32}H_{28}N_8Cl_2Cu$**
3.	Bis-pentanyl R(2-anisidine)- phenyldiazine Cu(II) bis-benzenediamine	Bisp(2-anisidine) pdCu(II)bisbd	**$C_{34}H_{32}N_8O_2Cl_2Cu$**
4.	Bis-pentanyl R(4-chloro)-phenyldiazine Cu(II) bis-benzenediamine	Bisp(4-chloro) pdCu(II)bisbd	**$C_{32}H_{26}N_8Cl_4Cu$**
5.	Bis-pentanyl R(4-Bromo)-phenyldiazine Cu(II) bis-benzenediamine	Bisp(4-Bromo) pdCu(II)bisbd	**$C_{32}H_{26}N_8Cl_2Br_2Cu$**
6.	Bis-pentanylR(2- chloro)-phenyldiazine Cu(II) bis-benzenediamine	Bisp(2-chloro) pdCu(II)bisbd	**$C_{32}H_{26}N_8Cl_4Cu$**
7.	Bis-pentanyl R(3-Nitro)-phenyldiazine Cu(II) bis-benzenediamine	Bisp(3Nitro)pdCu(II)bisbd	**$C_{32}H_{26}N_{10}O_4Cl_2Cu$**
8.	Bis-pentanyl R(2- Nitro)-phenyldiazine Cu(II) bis-benzenediamine	Bisp(2- Nitro) pdCu(II)bisbd	**$C_{32}H_{26}N_{10}O_4Cl_2Cu$**
9.	Bis-pentanyl R(4-anisidine)- phenyldiazine Cu(II) bis-benzenediamine	Bisp(4-anisidine) pdCu(II)bisbd	**$C_{32}H_{26}N_8Cl_4Cu$**
10.	Bis-pentanyl R(Aceto-p-Toludine)- phenyldiazine Cu(II) bis-benzenediamine	Bisp(Aceto-p-Toludine)pdCu(II)bisbd	**$C_{36}H_{32}N_8O_2Cl_2Cu$**

5.2 Experimental

The X-ray absorption spectra at the K-edge of copper of these mixed ligand copper complexes have been recorded at the Dispersive Extended X-ray Absorption Fine Structure (DEXAFS) beamline, which has been recently set-up by Applied Spectroscopy Division, BARC at the Indus-2 synchrotron radiation source at Raja Ramanna Centre for Advanced Technology (RRCAT), Indore[147].

The detailed description, features and calibration of the Dispersive Extended X-ray Absorption Fine Structure (DEXAFS) Beamline (BL-8) has already been given in chapter II and chapter IV of this thesis.

5.3 Results

In an XAFS experiment the incident and transmitted X-ray intensities are measured as a function of energy. The intensity of the x-ray after passing through a sample of thickness x is given by: $\mathbf{I_t = I_0 e^{-\mu x}}$, Where μ is the absorption coefficient and x is the thickness of the absorber, the absorption $\mu(E)$ corresponding to the photon energy (E).

The plot of absorption versus photon energy is obtained by recording the intensities I_0 and I_t, as the CCD outputs, without and with the sample, respectively, and the absorption coefficient $\boldsymbol{\mu}$ is obtained using above relation. The experimental data has been analyzed using the available computer software package Athena version 0.8.061. The various steps of the procedure of the analysis are given in figures 5.1 (for Cu metal)and in figures 5.2- 5.11 for copper complexes.

The absorption spectra of the copper metal and its complexes are shown in figure 5.1 - 5.11(a). The normalization process has already been described in previous chapter of this thesis. Figures 5.1 -5.11 (b) shows that the normalized absorption spectra with the pre-edge along zero, an edge step of one and the post-edge region oscillating around one for copper metal and copper complexes.

[147] Das N. C., Jha S. N., Bhattacharya D., Poswal A. K., Sinha A. K. and Mishra V. K., 2004, Sadhana, **29**, 5, 545. Bhattacharya D., Poswal A. K., Jha S. N., Sangeeta and Sabharwal S. C., 2009(a), Bull. Mater. Sci., **32**, 1, 103. Bhattacharyya D., Poswal A. K., Jha S. N., Sangeeta and Sabharwal S. C. 2009(b), Nucl. Instrum. Meth. A, **609**, 286

5.3.1 The absorption edge

Figures5.1-5.11 (c) indicating the positions of the absorption edge K and principal absorption maximum A in the region -30 > E > 50 eV of all copper complexes, in XAFS spectra. The values of E_K for the K-absorption edge of copper metal and its complexes studied are given in table 5.2. These have been determined as the energies of the first peak in the derivative spectra.

5.3.2 Position of the edge

In the region 30 > E > 50 eV, figures 5.1-5.11 (d) and shows that the first derivative of absorption spectra indicating the position of the absorption edges K and principal absorption maximum A. The K- absorption edge (E_K) described by the first peak i.e., the position of first inflection point in the derivative spectra. The position where the derivative is zero, gives the position of principal absorption maxima (E_A). The results of the energies of the K-absorption edge (E_K) and the energies of principal absorption maximum A (E_A) of copper in metal and its complexes are presented in table 5.2.

Figures 5.1-5.11 (e) shows that the EXAFS spectra converted into k space. The maxima and minima of the spectra for different values of K have been labeled with the conventional Latin and Greek alphabets respectively. The values of energy E and wave vector k corresponding to these maxima and minima have been given in table 5.3 (a) & (b) for copper metal and copper (II) complex.

5.3.3 Chemical shift

The chemical shift[148] and XAS studies[149] have been utilized to obtain important chemical information regarding the coordination in the complexes belonging to transitional metals .The K-absorption edge of copper has been found to be shifted

[148] Wakita H., Yamaguchi T., Yoshida N., and Fujiwara M., 1993, Jpn. J. Appl. Phys., **32**, 836.
Joshi S. K., Shrivastava B. D., and Mahajan N. K., 1997, J. Phys., **7**, C2-643.
Katare R. K., Joshi S. K., Shrivastava B. D., Pandeya K. B., and Mishra A., 2000, X-ray Spectrom., **29**, 187.
Katare R. K., Joshi S. K., Shrivastava B. D., Patel R. N. and Mishra A., 2002(a), Indian J. Pure and Appl. Phys., **40**, 908.
[149] Furenlid L. R., Renner M. W., and Fujita E., 1995, Physica B, **208 and 209**, 739.

towards the high energy side in all the complexes studied as compared to the K-absorption edge in the metal. The shifts of the K-absorption edge of copper in the complexes with respect to that of copper metal have been determined according to the eqn.

$$\Delta E_K = E_K \text{ (complex)} - E_K \text{ (metal)}$$

The results are given in table 5.4. For computing the chemical shift the value of E_K(Cu metal) has been taken as 8980.5 eV.

The compounds having copper in oxidation state in +1 show chemical shifts less than 5 eV while those having copper in oxidation state in +2 show chemical shifts more than 5 eV .In table 5.3, all the ten complexes have the values of chemical shifts between 5.06 to 11 eV. Hence, on the basis of values of the chemical shifts, all the complexes are found to have copper in oxidation state +2.

The chemical shift is largest for Bisp(Aceto-p-Toludine)pdCu(II)bisbd and the order for other complexes is as follows:

Bisp(Aceto-p-Toludine)pdCu(II)bisbd > Bisp(4-anisidine) pdCu(II)bisbd > Bisp(2-Nitro) pdCu(II)bisbd > Bisp(3Nitro)pdCu(II)bisbd > Bisp(2-chloro) pdCu(II)bisbd > Bisp(4-Bromo) pdCu(II)bisbd > Bisp(4-chloro) pdCu(II)bisbd > Bisp(2-anisidine) pdCu(II)bisbd > Bisp(pure anilene) pdCu(II)bisbd > Bisp(4-Nitro) pdCu(II)bisbd.

As is well known, an ionic bonding enhances the chemical shift, whereas a covalent bonding suppresses it. Hence, the above order may also be taken as representative of the relative ionic character of the bonding in these complexes.

5.3.4 Effective nuclear charge and Chemical Shift

Following Gianturco et al[150], Gupta and Nigam[151] and Nigam and Gupta[152] have outlined the method of determining the effective nuclear charge on ions from the measurement of the chemical shifts. The method has been outlined in section 4.3.4 of chapter IV of this thesis.

---

[150] Gianturco F. A. and Coulson C. A., 1968, Mol. Phys., **14**, 223

[151] Gupta M. K. and Nigam A. K., 1972(a), J. Phys. F, **2**, 1174.
Gupta M. K. and Nigam A. K., 1972(b), J. Phys. B, **5**, 1790

[152] Nigam A. K. and Gupta M. K., 1973, J. Phys., F **3**, 1251.
Nigam A. K. and Gupta M. K., 1974, J. Phys., F **4**, 1084

If the binding energies of K electron of copper in different oxidation states are determined, one can find from the difference in binding energies of the neutral atom and the ionized atom, the so called theoretical shifts in the X-ray absorption edge.
In the present work, the values of binding energies have been determined from the tables of Clementi and Roetti[153] using Koopman's theorem[154]. The values of these binding energies and the theoretical shifts for copper are given in table 4.5in chapter IV of this thesis.

The theoretical shifts are plotted against the oxidation number. Such a graph for copper atom is shown in fig.4.9 in chapter IV of this thesis. This graph has been obtained by fitting a third order polynomial to the points. The polynomial and the parameters are given in table 4.7. in chapter IV of this thesis.

From this graph, the effective nuclear charge on copper in its complexes has been determined and the results have been presented in table 5.2.

5.3.5 Principal absorption maximum

In table 5.2, we have also included the data for the principal absorption maximum E_A for the complexes. It has been observed that with respect to copper metal, the value of E_A is shifted towards the higher energy side. The reason for the shift of the principal absorption maximum to the higher energy side has already been discussed in section 1.7.1(b).

For the complexes mentioned in table 5.1, the energy range of chemical shift in these complexes is between 5.06-11 eV while the range for shift of principal absorption maximum is between 8.5-18.93 eV. Hence, on the basis of the shift of the principal absorption maximum also it can be inferred that copper is in +2 oxidation state in these complexes.

The shift of the principal absorption maximum for Cu (II) complexes are in the order:

Bisp(4-Nitro)pdCu(II)bisbd > Bisp(pureanilene)pdCu(II)bisbd > Bisp(2-anisidine) pdCu(II)bisbd > Bisp(4-chloro) pdCu(II)bisbd > Bisp(4-Bromo) pdCu(II)bisbd > Bisp(2-chloro) pdCu(II)bisbd > Bisp(3Nitro)pdCu(II)bisbd > Bisp(2-

[153]Clementi E. and Roetti C., 1974, Atomic data and Nuclear data tables, **14**, 177.
Koopmans T., 1934, Physica, **1**, 104.
[154] Koopmans T., 1934, Physica, **1**, 104.

Nitro) pdCu(II)bisbd > Bisp(4-anisidine) pdCu(II)bisbd > Bisp(Aceto-p-Toludine)pdCu(II)bisbd.

The order of the shift of the principal absorption maximum is in the reverse order of chemical shift of the complexes except that the shift for Bisp(2-chloro) pdCu(II)bisbd . This represents that the shift of the principal absorption maximum is inversely proportional to ionic character for this series.

5.3.6 Edge-width

In table 5.2, the values of the edge-width (E_A-E_K) have been reported. The experimental data of edge-width of Cu (II) complexes (Table 5.2) show that the order of edge-width is as follows:

Bisp(4-Nitro)pdCu(II)bisbd > Bisp(pure anilene)pdCu(II)bisbd > Bisp(2-anisidine) pdCu(II)bisbd > Bisp(3-toludine)pdCu(II)bisbd > Bisp(4-chloro)pdCu(II)bisbd > Bisp(4-Bromo) pdCu(II)bisbd > Bisp(2-chloro) pdCu(II)bisbd > Bisp(3Nitro)pdCu(II)bisbd > Bisp(2-Nitro) pdCu(II)bisbd > Bisp(4-anisidine) pdCu(II)bisbd > Bisp(Aceto-p-Toludine)pdCu(II)bisbd

The order of the edge-width is in the reverse order of chemical shift of the same complexes. This represents that the edge-width is inversely proportional to ionic character for this series. The reverse trend for these complexes is justified on the basis of the criterion that, in general, edge-width of the K-absorption edge increases with the increase of covalent character of the bonds provided other factors like molecular symmetry etc., remain the same[155]. The reverse trend is justified on this basis.

5.3.7 Determination of bond lengths

5.3.7.1 (i) By graphical methods from EXAFS spectra

The EXAFS appearing on high energy side of the K-absorption edge have been recorded in all the copper complexes, studied in this chapter, using the synchrotron DEXAFS beamline set-up. Following the principal absorption maxima, there are distinct EXAFS features, extending up to 350 eV on the high energy side of the K-

[155] Kumar A., Nigam A. N. and Shrivastava B. D., 1981, X-ray Spectrom., **10**, 25

absorption edge. The profiles of the K-absorption discontinuity along with fine structure for copper metal and all the complexes are shown in figs. (a) of 5.1 - 5.11.

The inflection point on the K-edge (i.e., K1 edge) is taken as the reference point for the measurement of the extended fine structure. The positions of the EXAFS maxima and minima in eV and their corresponding values of k in $\mathring{A}^{-1}$ are given in table 5.3 (a) & (b).

The Fourier transformation technique mentioned in section 1.9.2 can be used for determination of the bond lengths. Hence, in the present thesis, bond length has been determined by the Fourier transformation method for the copper complexes and copper complexes studied in this chapter and in chapter IV. However, only the phase uncorrected bond length has been determined by this method. No attempt has been made to employ the fitting procedures by which phase corrected bond length can be determined, because the required crystallographic data is not available for any of the complexes studied.

The bond length can also be determined from EXAFS data by three graphical methods mentioned in section 1.9.1. In fact before the Fourier transformation technique was formulated, the bond length used to be extracted from the EXAFS data by the three graphical methods. We have used all the three methods for determination of bond lengths in copper complexes studied in the present thesis.

Thus, the bond lengths have been determined for the copper complexes with the help of three methods, i.e., Levy's (1965) Lytle's (1966) and Lytle, Sayers and Stern's (L.S.S.) (1975) methods and the results are given in table 5.4. These methods have already been described in detail in section 1.9.1 and are briefly mentioned below.

5.3.7.1.1 (a) Levy's method[156]

In Levy's method, the bond lengths are calculated by using the relation:

$$R_1 = [151/\Delta E]^{1/2} \text{ Å},$$

where ΔE is the difference in eV of the energies of the EXAFS maximum B and minimum β and R_1 is the radius of the first coordination sphere. The positions of B

[156] Levy R. M., 1965, J. Chem. Phys., **43**, 1846.

and β are given in table 5.3 (a) & (b) for the complexes. The bond lengths thus determined are given in table 5.4.

5.3.7.1.2 (b) Lytle's method[157]

The energy values (E) of the EXAFS maxima, given in table 5.3 (a) & (b), are plotted against the Q values given by Lytle for p symmetry, i.e., Q = 2.04, 6.0, 12.0, and 20.0. The (E, Q) plots have been found to be linear and are given in figs. 5.8. The slope M of the E versus Q plots have been used to evaluate the radius R_s of equivalent polyhedron, by using the relation (1.13), i.e., $R_S = [37.60 / M]^{1/2}$. The values of R_s calculated with the help of this method are reported in table 5.4 for all the complexes. It may be remarked here that Levy's method gives the radius of coordination sphere directly where as Lytle's method does not. In the later method, the interatomic spacing is obtained by multiplying R_s with a factor appropriate to the geometry of the system.

5.3.7.1.3 (c) L.S.S. method[158]

The values of the wave vector k ($Å^{-1}$) for EXAFS maxima (n = 0, 2, 4....) and minima (n =1, 3, 5....), for all the copper complexes, are presented in table 5.3 (a) & (b). In the Lytle, Sayers and Stern's (L.S.S.) method for determination of the nearest neighbour distances, n versus k graph is plotted. The plots have been found to be linear for all the complexes and are shown in figs 5.9. The slope of n versus k plot, gives the value of $2(R_1 - \alpha_1) / \pi$ where R_1 is the bond length (eqn. 1.19). The parameter α_1 depends to a large extent on the central absorbing atom[159]. It is found that for chemically similar system, the values of α_1 remains more or less the same. The values of $(R_1 - \alpha_1)$ thus obtained are given in table 5.4.

5.3.7.2 (ii) By Fourier transform of EXAFS spectra

[157] Lytle F.W., 1966, Advances in X-ray Analysis, **9**,398.
[158] Lytle F. W., Sayers D. E. and Stern E. A., 1975(a), Phys. Rev. B, **11,** 4825
[159] Lytle F.W., 1966, Advances in X-ray Analysis, **9**,398

As has been described in section 1.9.2 of chapter I of this thesis, the Fourier transform of the $\chi(k)$ versus k spectra peaks at the radial distances of the neighboring atoms from the absorbing atom. However, the distance found from Fourier transform is about 0.2 Å - 0.5 Å shorter than the actual distance due to energy dependence of the phase factors in the sine function of the EXAFS equation (1.10). The peaks in the Fourier transform are shifted towards the origin by an amount α_j and hence the peaks are at distances $R_j-\alpha_j$[160]. For the first peak j=1 and hence the position of the first peak determines the distance $R_1-\alpha_1$. This method has already been described in detail in chapter-I of this thesis.

It is important to note here that the distance $R_1-\alpha_1$ should be equal to the distance found from the L.S.S. graphical method outlined above. Hence, both the L.S.S. method and the Fourier transformation method give the value $R_1-\alpha_1$, i.e., both the methods give the value of bond lengths which have not been corrected for the phase shifts. We have called this distance as the phase uncorrected bond length.

The normalized spectra shown in figures (b) of 5.1 - 5.11 are $\mu(E)$ versus E curves obtained using the synchrotron DEXAFS beamline set-up. From these curves, $\chi(k)$ versus k curves are obtained which are given in figs. (e) of 5.1 - 5.11. The Fourier transformed spectra obtained from $\chi(k)$ versus k curves are given in figures (f) of 5.1 - 5.11. The position of the first peak in the Fourier transform gives the value of $R_1-\alpha_1$ and the values are collected in table 5.4 for all the complexes.

It is seen from this table that the value of $R_1-\alpha_1$ as determined from L.S.S. method and that determined from the Fourier transformation method are in good agreement with each other, i.e., both the L.S.S. method and Fourier transformation method give nearly the same value of the phase uncorrected bond length, i.e., $R_1-\alpha_1$.

5.4 Conclusions

The conclusions drawn in this chapter are as follows:

- X-ray absorption spectra of copper complexes at the K-edge of copper have been recorded at the recently developed EXAFS beamline set-up at the Indus-2 synchrotron source at RRCAT, Indore.

[160] Stern E. A., Sayers D. E. and Lytle F. W., 1975, Phys. Rev. B, **11**, 4836.

- The K- absorption edge has been found in all copper complexes. The energies of K- edge (E_K), the values of chemical shifts, the principal absorption maxima (E_A) and EXAFS maxima and minima have been reported.

- The shift of the K-edge (chemical shift) has been obtained for all copper complexes. All the complexes have the values of chemical shifts between 5.06-11 eV. The complex Bisp(Aceto-p-Toludine)pdCu(II)bisbd is showing highest chemical shift, hence, it should have the maximum ionic character amongst the studied complexes. The values of the chemical shifts suggest that copper is in oxidation state +2 in all of the complexes. The order of the chemical shift is as follows:

- Bisp(Aceto-p-Toludine)pdCu(II)bisbd > Bisp(4-anisidine) pdCu(II)bisbd > Bisp(2-Nitro) pdCu(II)bisbd > Bisp(3Nitro)pdCu(II)bisbd > Bisp(2-chloro) pdCu(II)bisbd > Bisp(4-Bromo) pdCu(II)bisbd > Bisp(4-chloro) pdCu(II)bisbd > Bisp(2-anisidine) pdCu(II)bisbd > Bisp(pure anilene) pdCu(II)bisbd > Bisp(4-Nitro) pdCu(II)bisbd.

- The values of shift of the principal absorption maximum have been obtained for all copper complexes. The order of shift of principal absorption maximum for all the complexes is in reverse order of the chemical shift. The reverse order represents that the shift of the principal absorption maximum is inversely proportional to ionic character for the complexes. The complex Bisp(4-Nitro) pdCu(II)bisbd is showing highest values of shift of principal absorption maxima.

- The chemical shift has been used to determine the effective nuclear charge on the absorbing atom.

- The edge-width has also been studied for all the complexes. The order of the edge-width is in the reverse order of chemical shift of the complexes. The reverse order represents that the edge-width is inversely proportional to ionic character for this series.

- From the positions of the EXAFS maxima and minima, the bond lengths in the complexes have been determined by three different methods viz. Levy's, Lytle's and Lytle, Sayers and Stern's (L.S.S.) methods.

- The normalized spectra, i.e., μ (E) versus E curves have been obtained. From these curves, $\chi(k)$ versus k curves have been obtained, which have then been Fourier transformed using the software Athena. From the Fourier transforms of the EXAFS spectra the bond lengths have been determined.

- It has been observed that the value of the phase uncorrected bond length, i.e., R_1-α_1 as determined from L.S.S. method and that determined from the Fourier transformation method are in good agreement with each other, i.e., both the L.S.S. method and Fourier transformation method give nearly the same value of the phase uncorrected bond length.

Table 5.2 XANES data for K-absorption edge of Copper (II) complexes.						
Complexes	**E_K (eV)**	**E_A (eV)**	**Chemical shift $\Delta E_K = (E_{complex} - E_{metal})$ (eV)**	**ENC**	**Shift of the principal absorption maximum (eV)**	**Edge-width $(E_A - E_k)$ (eV)**
Cu Metal	**8980.5**	**8995.06**	-	-	-	**8.6**
Bisp(4-Nitro)pdCu(II)bisbd	**8985.5**	**9004.50**	**5.0**	**.65**	**9.4**	**18.9**
Bisp(pureanilene)pdCu(II)bisbd	**8986.9**	**9003.74**	**6.2**	**.73**	**8.6**	**16.8**
Bisp(2-anisidine)pdCu(II)bisbd	**8986.7**	**9000.70**	**6.6**	**.75**	**5.6**	**13.9**
Bisp(4-chloro) pdCu(II)bisbd	**8988.1**	**9000.30**	**7.6**	**.85**	**5.2**	**12.2**
Bisp(4-Bromo) pdCu(II)bisbd	**8988.3**	**9000.20**	**7.8**	**.87**	**5.1**	**11.9**
Bisp(2-chloro) pdCu(II)bisbd	**8988.4**	**9000.15**	**7.9**	**.88**	**3.9**	**10.5**
Bisp(3-Nitro)pdCu(II)bisbd	**8989.2**	**9000.10**	**8.7**	**.95**	**5.0**	**10.8**
Bisp(2-Nitro) pdCu(II)bisbd	**8989.9**	**9000.00**	**9.4**	**.98**	**4.9**	**10.0**
Bisp(4-anisidine)pdCu(II)bisbd	**8990.9**	**9000.00**	**10.4**	**1.03**	**4.9**	**9.0**
Bisp(AcetoToludine)pdCu(II)bisbd	**8991.5**	**9000.00**	**11.0**	**1.06**	**4.9**	**8.5**

Table 5.3 EXAFS Parameter for Cu (II) complex

Table 5.3 (a) EXAFS Parameter for Cu (II) complex (1-5)												
Structure	**n**	**Q**	**Cu1**		**Cu2**		**Cu3**		**Cu4**		**Cu 5**	
			E (eV)	**k ($Å^{-1}$)**	**E (eV)**	**k ($Å^{-1}$)**	**E (eV)**	**k ($Å^{-1}$)**	**E (eV)**	**k ($Å^{-1}$)**	**E (eV)**	**k ($Å^{-1}$)**
A	**0**	**2.04**	**13.3**	**1.87**	**18.2**	**2.19**	**13.3**	**1.87**	**13.3**	**1.87**	**5.3**	**1.18**
α	**1**	**-**	**45.7**	**3.50**	**41.1**	**3.29**	**46.5**	**3.50**	**45.7**	**3.50**	**30.4**	**2.83**
B	**2**	**6.04**	**97.3**	**5.02**	**60.8**	**4.0**	**95.8**	**5.02**	**97.3**	**5.02**	**48.1**	**3.56**
β	**3**	**-**	**162.1**	**6.53**	**106.4**	**5.29**	**162.1**	**6.53**	**162.1**	**6.53**	**126.5**	**5.77**
C	**4**	**12**	**190.6**	**7.10**	**158.1**	**6.45**	**191.6**	**7.10**	**190.6**	**7.10**	**155.7**	**6.4**
γ	**5**	**-**	**289.1**	**8.63**	**198.2**	**7.22**	**285.8**	**8.67**	**289.1**	**8.63**	**187.3**	**7.02**
D	**6**	**20**	**443.4**	**10.80**	**285.1**	**8.66**	**443.4**	**10.8**	**443.4**	**10.8**	**209.3**	**7.42**
δ	**7**	**-**	**487.2**	**11.32**	**-**	**-**	**487.2**	**11.3**	**487.2**	**11.32**	**487.2**	**11.32**

Table 5.3 (b) EXAFS Parameter for Cu (II) complexes (6-10)												
Structure	**n**	**Q**	**Cu6**		**Cu7**		**Cu8**		**Cu9**		**Cu10**	
			E (eV)	**k (Å^{-1})**	**E (eV)**	**k (Å^{-1})**	**E (eV)**	**k (Å^{-1})**	**E (eV)**	**k (Å^{-1})**	**E (eV)**	**k (Å^{-1})**
A	**0**	**2.04**	**13.1**	**1.86**	**13.1**	**1.86**	**15.20**	**2.00**	**13.2**	**1.87**	**13.1**	**1.86**
α	**1**		**32.8**	**2.94**	**35.5**	**2.97**	**33.53**	**2.97**	**46.5**	**3.50**	**35.5**	**2.97**
B	**2**	**6.04**	**58.1**	**3.91**	**58.3**	**3.94**	**58.72**	**3.93**	**97.3**	**5.06**	**58.32**	**3.94**
β	**3**		**123.5**	**5.7**	**116.2**	**5.53**	**123.5**	**5.7**	**164.1**	**6.57**	**116.2**	**5.53**
C	**4**	**12**	**154.7**	**6.38**	**154.7**	**6.38**	**155.2**	**6.39**	**192.4**	**7.12**	**154.7**	**6.38**
γ	**5**		**183.1**	**6.94**	**183.1**	**6.94**	**190.2**	**7.07**	**291.1**	**8.75**	**183.1**	**6.94**
D	**6**	**20**	**213.8**	**7.5**	**210.4**	**7.44**	**285.1**	**8.62**	**448.6**	**10.90**	**210.4**	**7.44**
δ	**7**		**13.1**	**1.86**	**13.1**	**1.86**	**15.20**	**2.00**	**490.6**	**11.36**	**13.1**	**1.86**

Table 5.4 Values of first shell bond lengths (in Å) calculated from Levy's, Lytle's, L.S.S. and Fourier transform methods for copper (II) complexes.					
S. No.	**Cu(II)Complexes**	**Phase corrected**		**Phase uncorrected**	
		Levy's method R_1	**Lytle's method R_s**	**L.S.S. method R_1-α_1**	**F.T. method R**
1	Bisp(4-Nitro)pdCu(II)bisbd	**1.50**	**1.27**	**1.12**	**1.10**
2	Bisp(pureanilene)pdCu(II)bisbd	**1.82**	**1.57**	**1.56**	**1.43**
3	Bisp(2-anisidine)pdCu(II)bisbd	**1.50**	**1.26**	**1.106**	**1.17**
4	Bisp(4-chloro) pdCu(II)bisbd	**1.52**	**1.26**	**1.104**	**1.11**
5	Bisp(4-Bromo) pdCu(II)bisbd	**1.38**	**1.78**	**1.31**	**1.32**
6	Bisp(2-chloro) pdCu(II)bisbd	**1.51**	**1.55**	**1.31**	**1.30**
7	Bisp(3-Nitro)pdCu(II)bisbd	**1.61**	**1.82**	**1.34**	**1.32**
8	Bisp(2-Nitro) pdCu(II)bisbd	**1.52**	**1.56**	**1.34**	**1.29**
9	Bisp(4-anisidine)pdCu(II)bisbd	**1.50**	**1.25**	**1.09**	**1.16**
10	Bisp(AcetoToludine)pdCu(II)bisbd	**1.50**	**1.27**	**1.10**	**1.16**

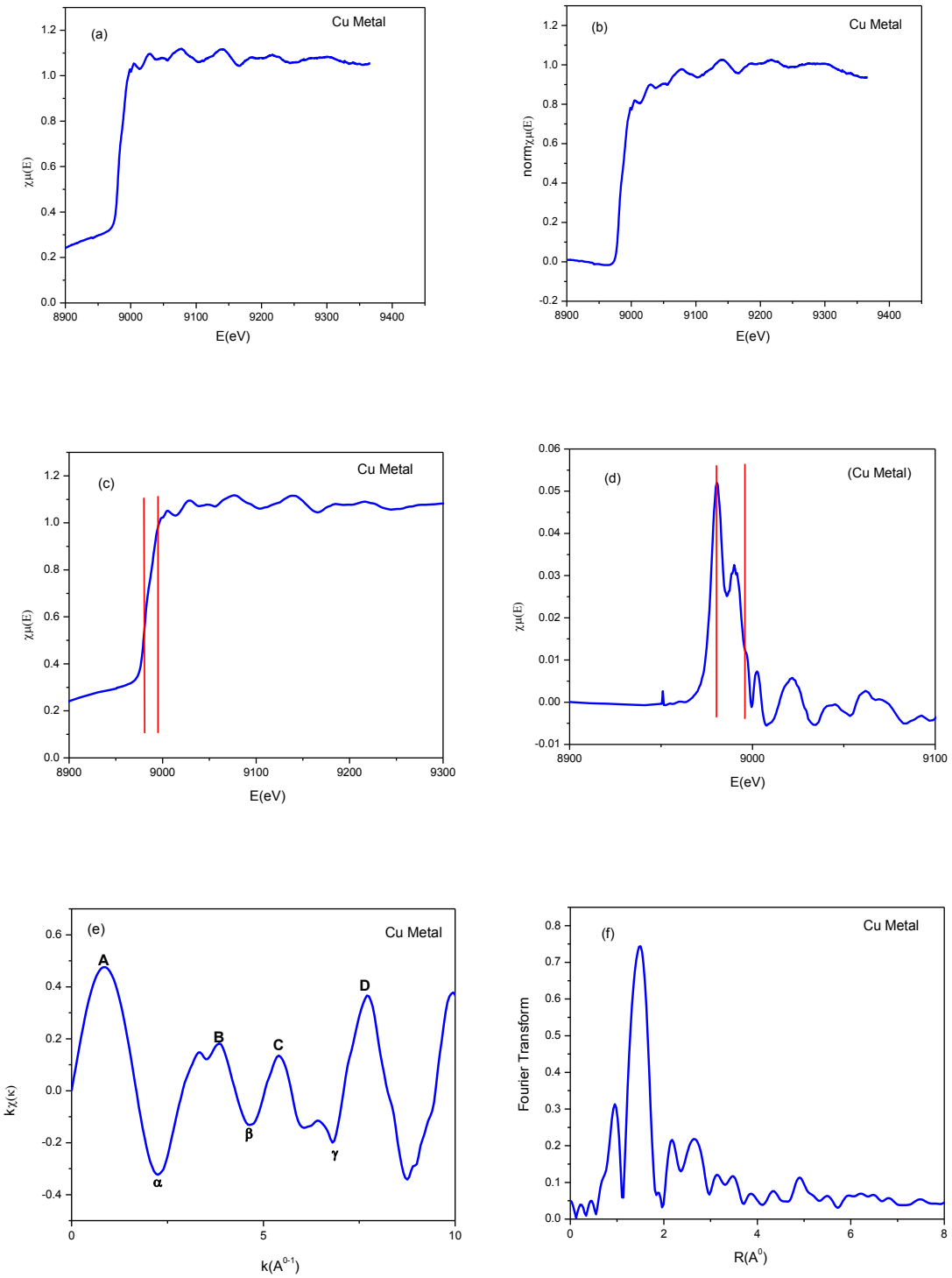

Figure 5-1 XAFS data analysis curves for copper metal

(a) Raw absorption versus photoelectron energy (b) The normalized absorption spectrum (c) XAFS spectrum and (d) Derivative of XAFS spectrum for copper metal indicating position of absorption edge K and principal absorption maxima A. (e) χ(k) versus k curve and (f) Magnitude of Fourier transform of the χ(k) versus k curve.

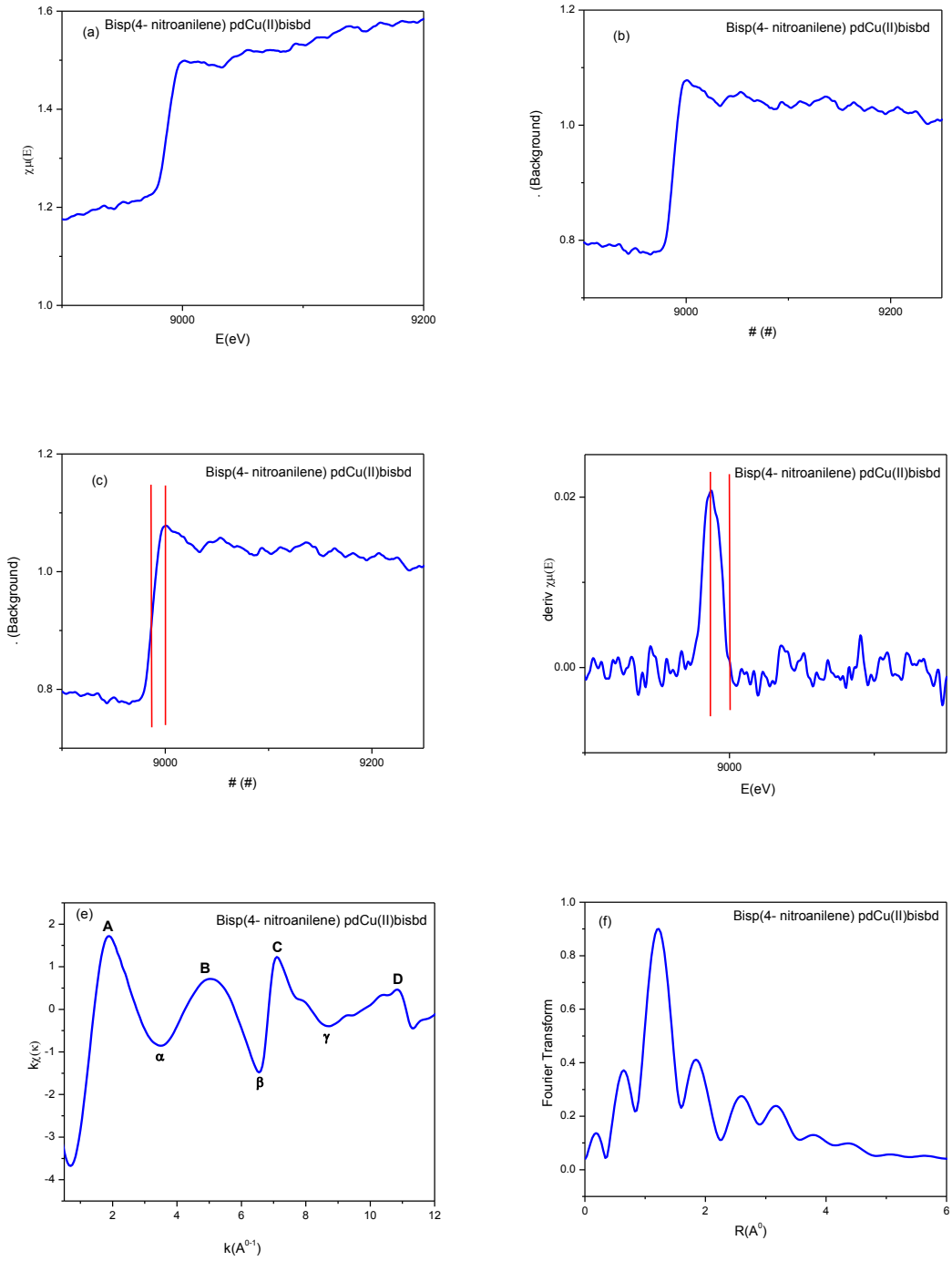

Figure 5-2 XAFS data analysis curves for Bisp(4- Nitro) pdCu(II)bisbd.

(a) Raw absorption versus photoelectron energy (b) The normalized absorption spectrum (c) XAFS spectrum and (d) Derivative of XAFS spectrum for copper metal indicating position of absorption edge K and principal absorption maxima A. (e) χ(k) versus k curve and (f) Magnitude of Fourier transform of the χ(k) versus k curve.

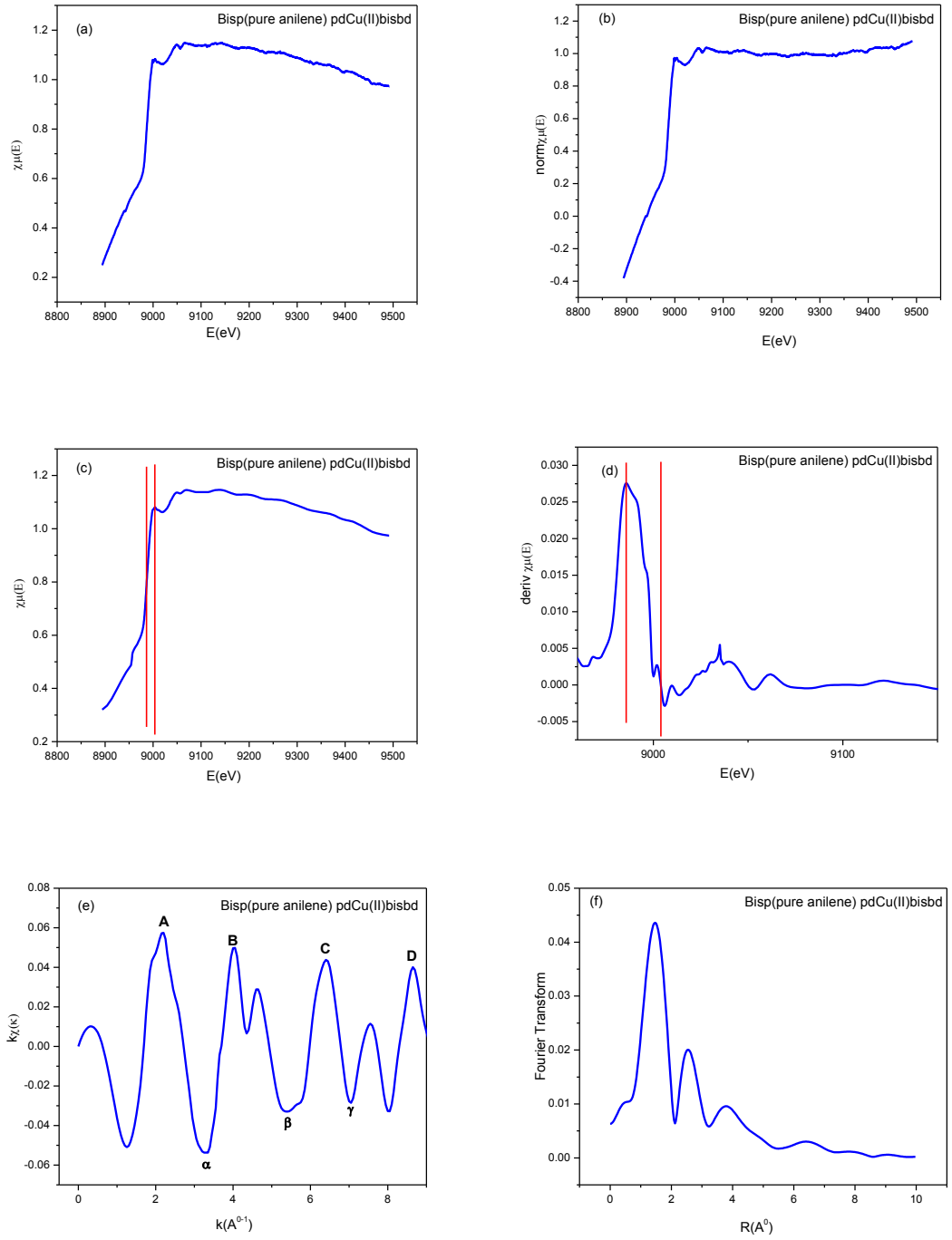

Figure 5-3 XAFS data analysis curves for Bisp(Pure anilene) pdCu(II)bisbd.

(a) Raw absorption versus photoelectron energy (b) The normalized absorption spectrum (c) XAFS spectrum and (d) Derivative of XAFS spectrum for copper metal indicating position of absorption edge K and principal absorption maxima A. (e) χ(k) versus k curve and (f) Magnitude of Fourier transform of the χ(k) versus k curve.

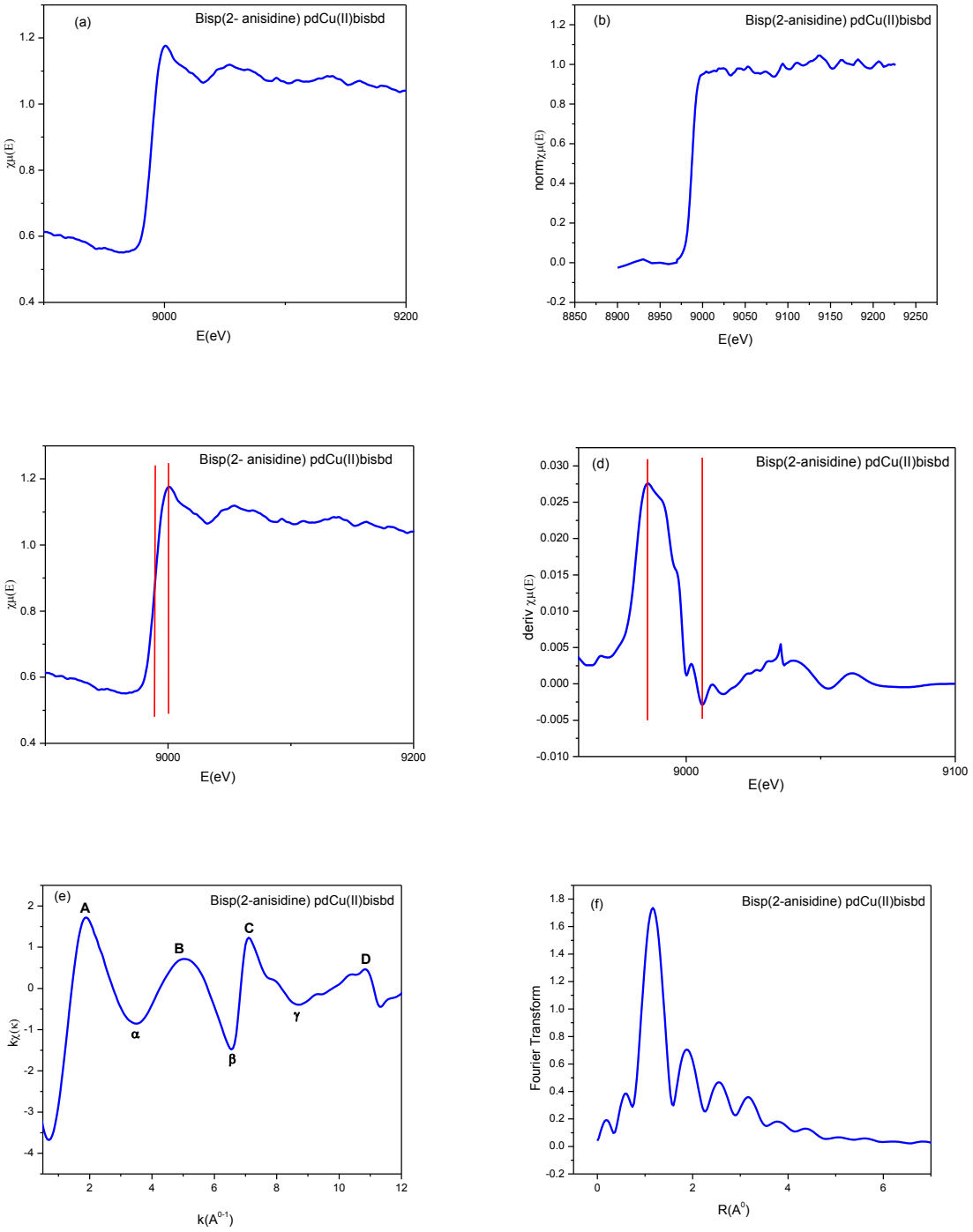

Figure 5-4 XAFS data analysis curves for Bisp(2-anisidine) pdCu(II)bisbd.

(a) Raw absorption versus photoelectron energy (b) The normalized absorption spectrum (c) XAFS spectrum and (d) Derivative of XAFS spectrum for copper metal indicating position of absorption edge K and principal absorption maxima A. (e) χ (k) versus k curve and (f) Magnitude of Fourier transform of the χ(k) versus k curve.

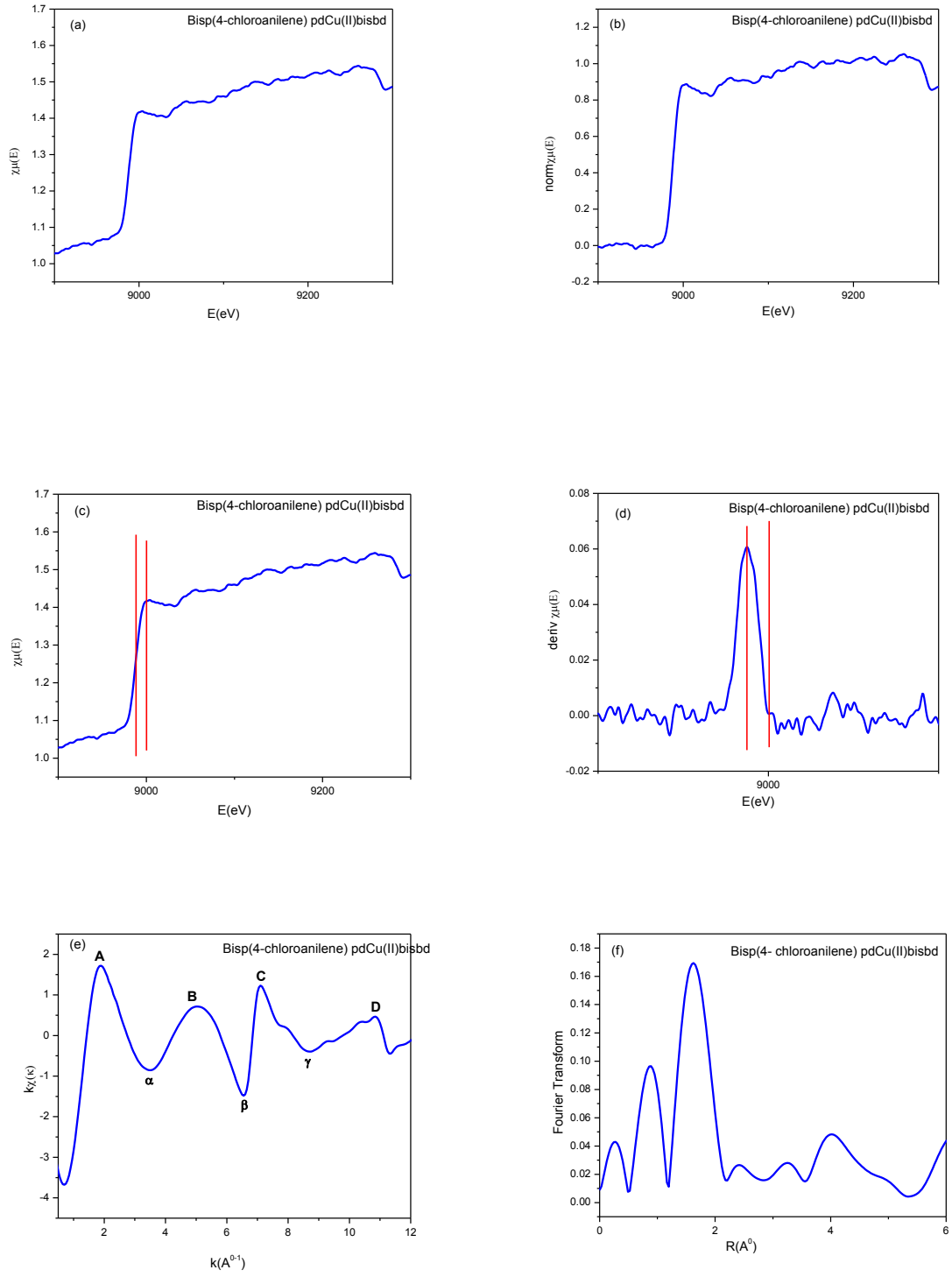

Figure 5-5 XAFS data analysis curves Bisp(4-chloroanilene) pdCu(II)bisbd.

(a)Raw absorption versus photoelectron energy (b) The normalized absorption spectrum (c) XAFS spectrum and (d) Derivative of XAFS spectrum for copper metal indicating position of absorption edge K and principal absorption maxima A. (e) χ (k) versus k curve and (f) Magnitude of Fourier transform of the χ(k) versus k curve.

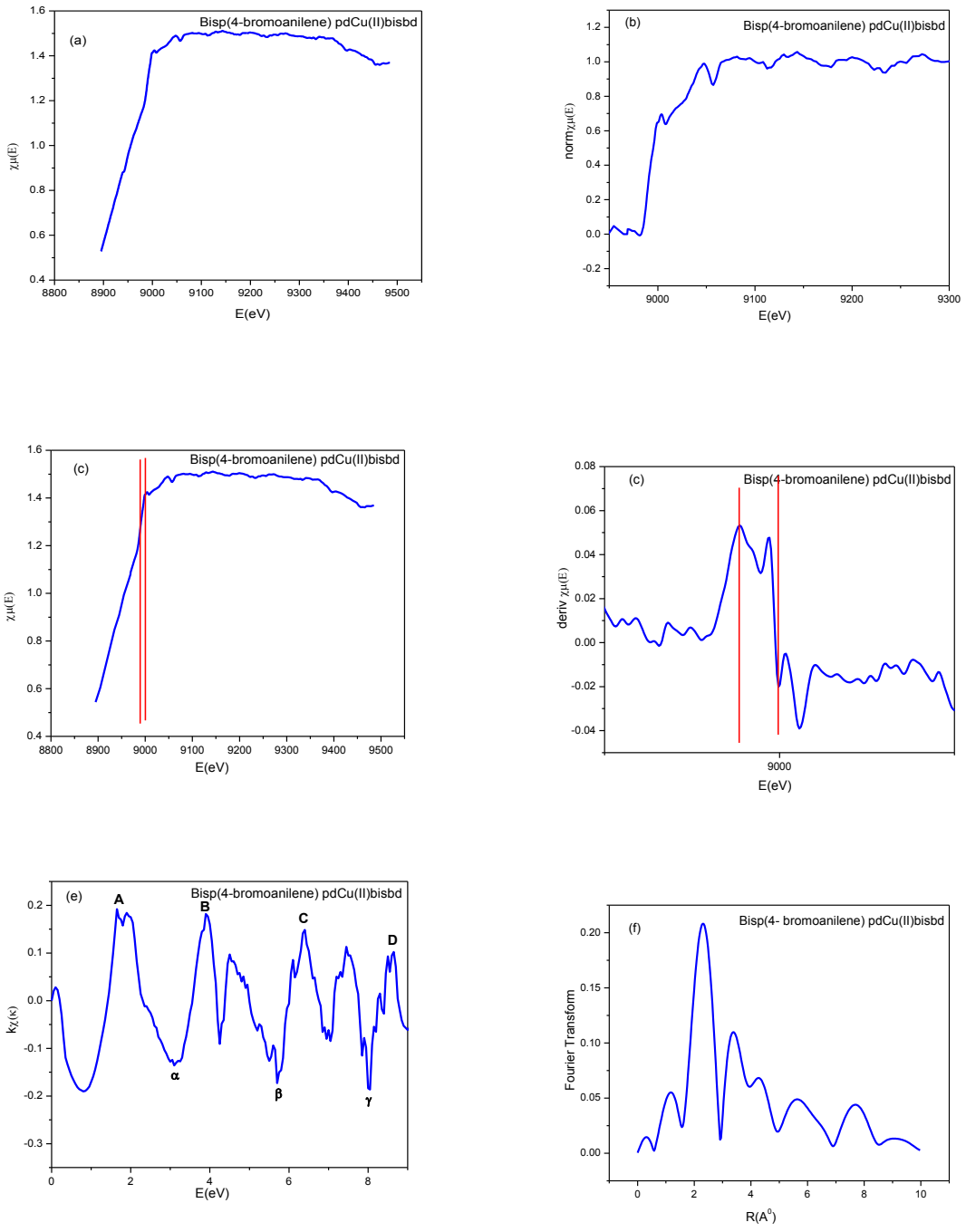

Figure 5-6 XAFS data analysis curves for Bisp(4-bromoanilene) pdCu(II)bisbd.

(a)Raw absorption versus photoelectron energy (b) The normalized absorption spectrum (c) XAFS spectrum and (d) Derivative of XAFS spectrum for copper metal indicating position of absorption edge K and principal absorption maxima A. (e) χ (k) versus k curve and (f) Magnitude of Fourier transform of the χ(k) versus k curve.

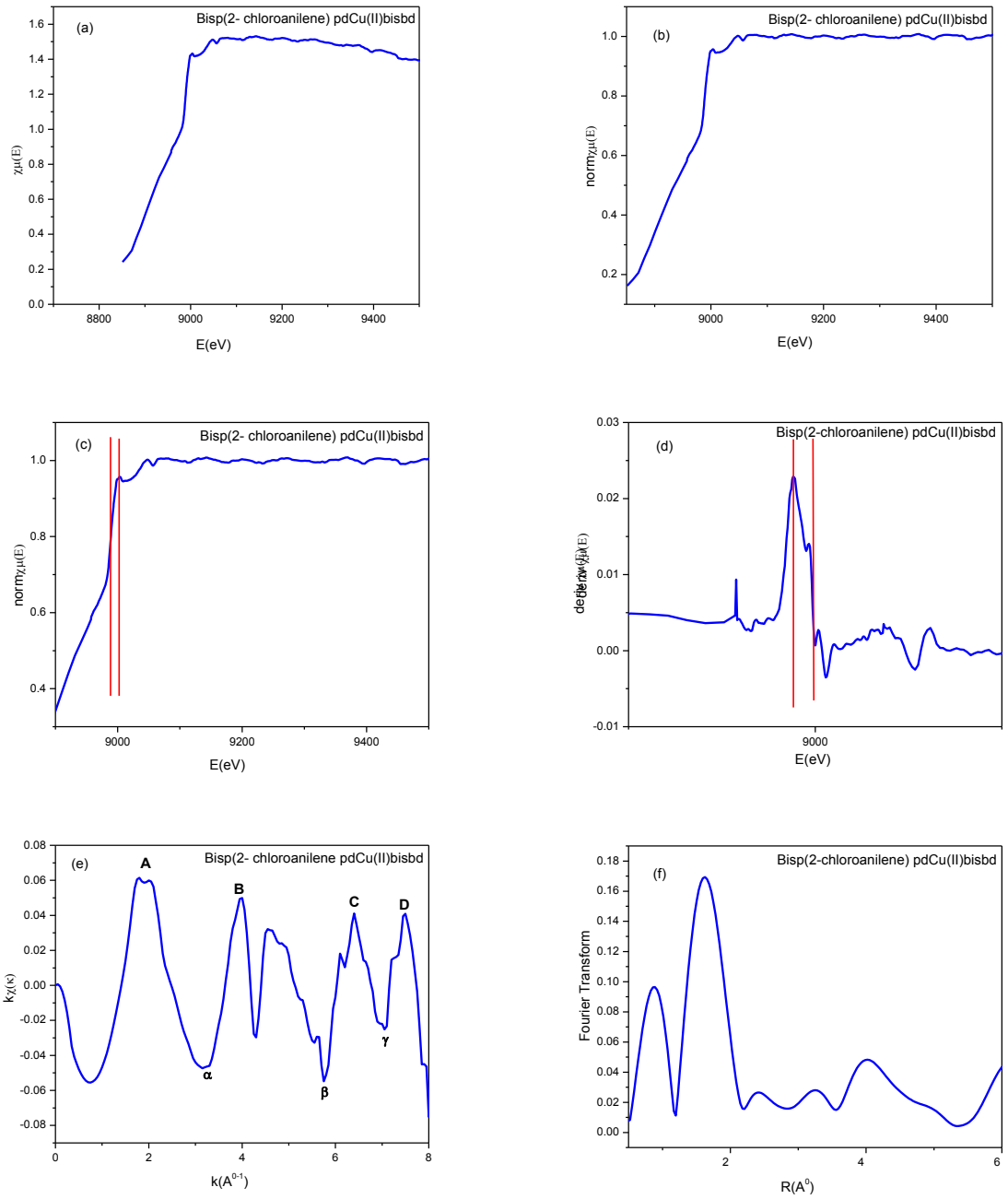

Figure 5-7 XAFS data analysis curves for Bisp(2-chloroanilene) pdCu(II)bisbd.

(a)Raw absorption versus photoelectron energy (b) The normalized absorption spectrum (c) XAFS spectrum and (d) Derivative of XAFS spectrum for copper metal indicating position of absorption edge K and principal absorption maxima A. (e) χ (k) versus k curve and (f) Magnitude of Fourier transform of the χ(k) versus k curve.

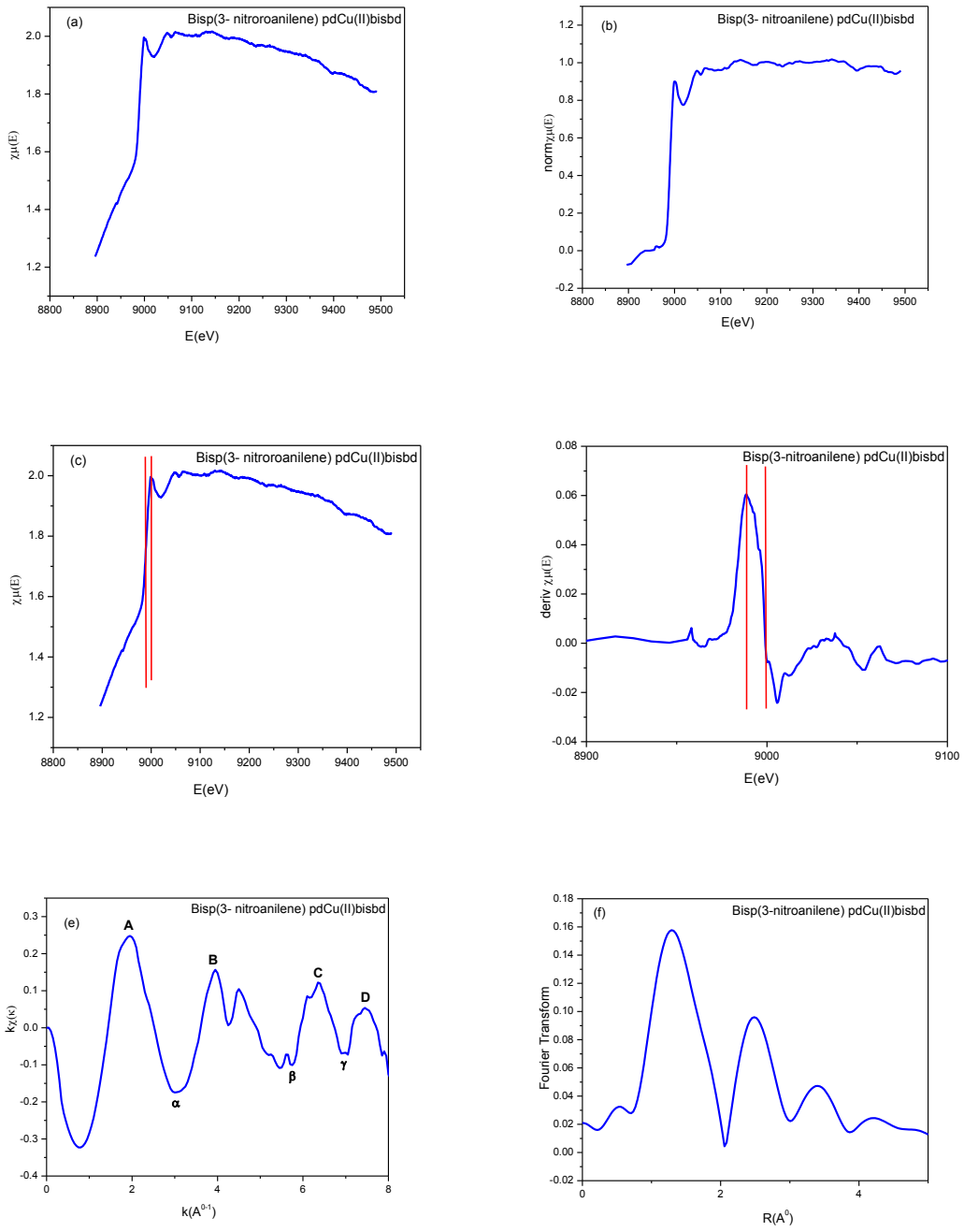

Figure 5-8 XAFS data analysis curves for Bisp(3-nitroanilene) pdCu(II)bisbd.

(a) Raw absorption versus photoelectron energy (b) The normalized absorption spectrum (c) XAFS spectrum and (d) Derivative of XAFS spectrum for copper metal indicating position of absorption edge K and principal absorption maxima A. (e) χ(k) versus k curve and (f) Magnitude of Fourier transform of the χ(k) versus k curve.

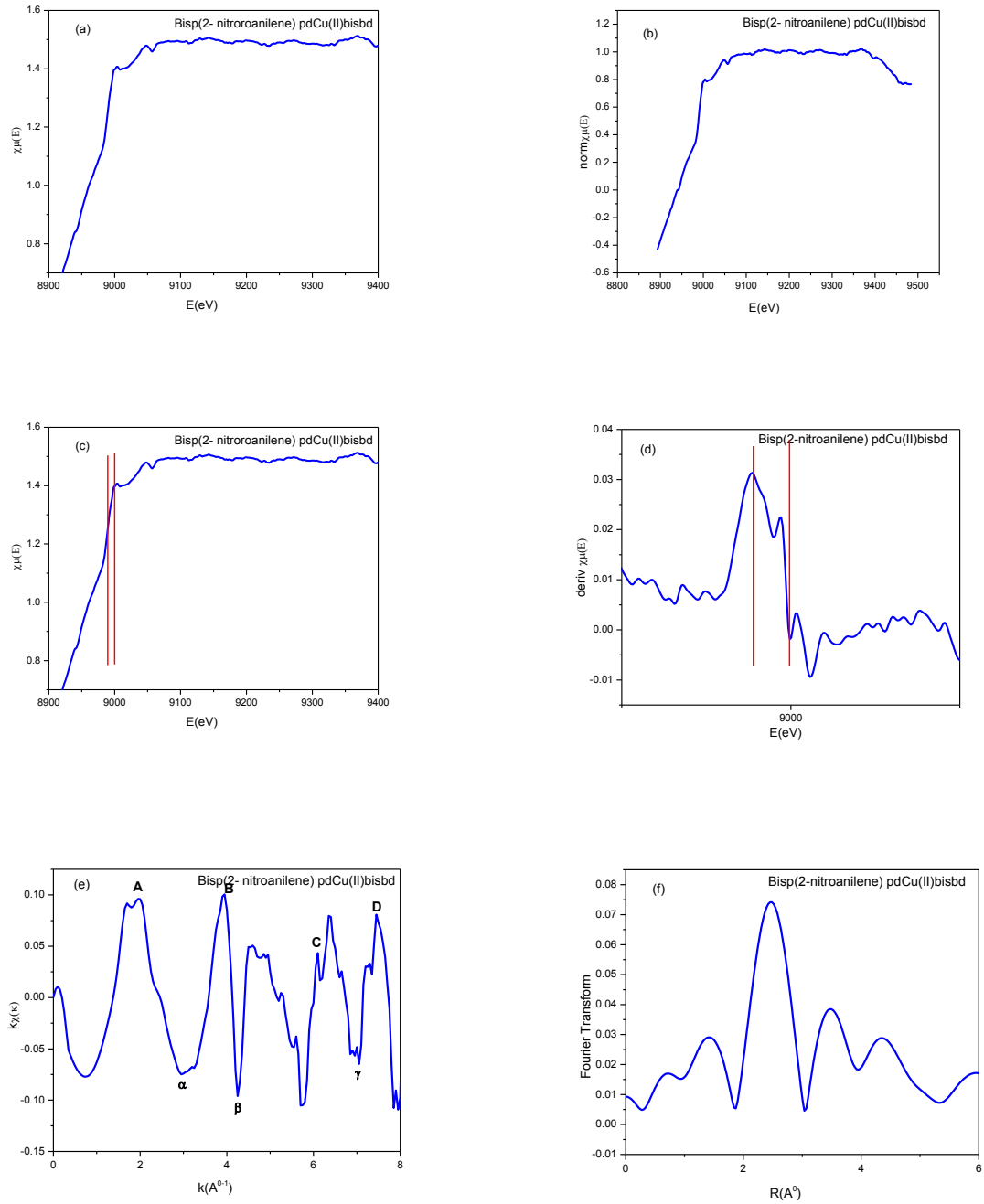

Figure 5-9 XAFS data analysis curves for Bisp(2-nitroanilene) pdCu(II)bisbd.

(a) Raw absorption versus photoelectron energy (b) The normalized absorption spectrum (c) XAFS spectrum and (d) Derivative of XAFS spectrum for copper metal indicating position of absorption edge K and principal absorption maxima A. (e) χ(k) versus k curve and (f) Magnitude of Fourier transform of the χ(k) versus k curve.

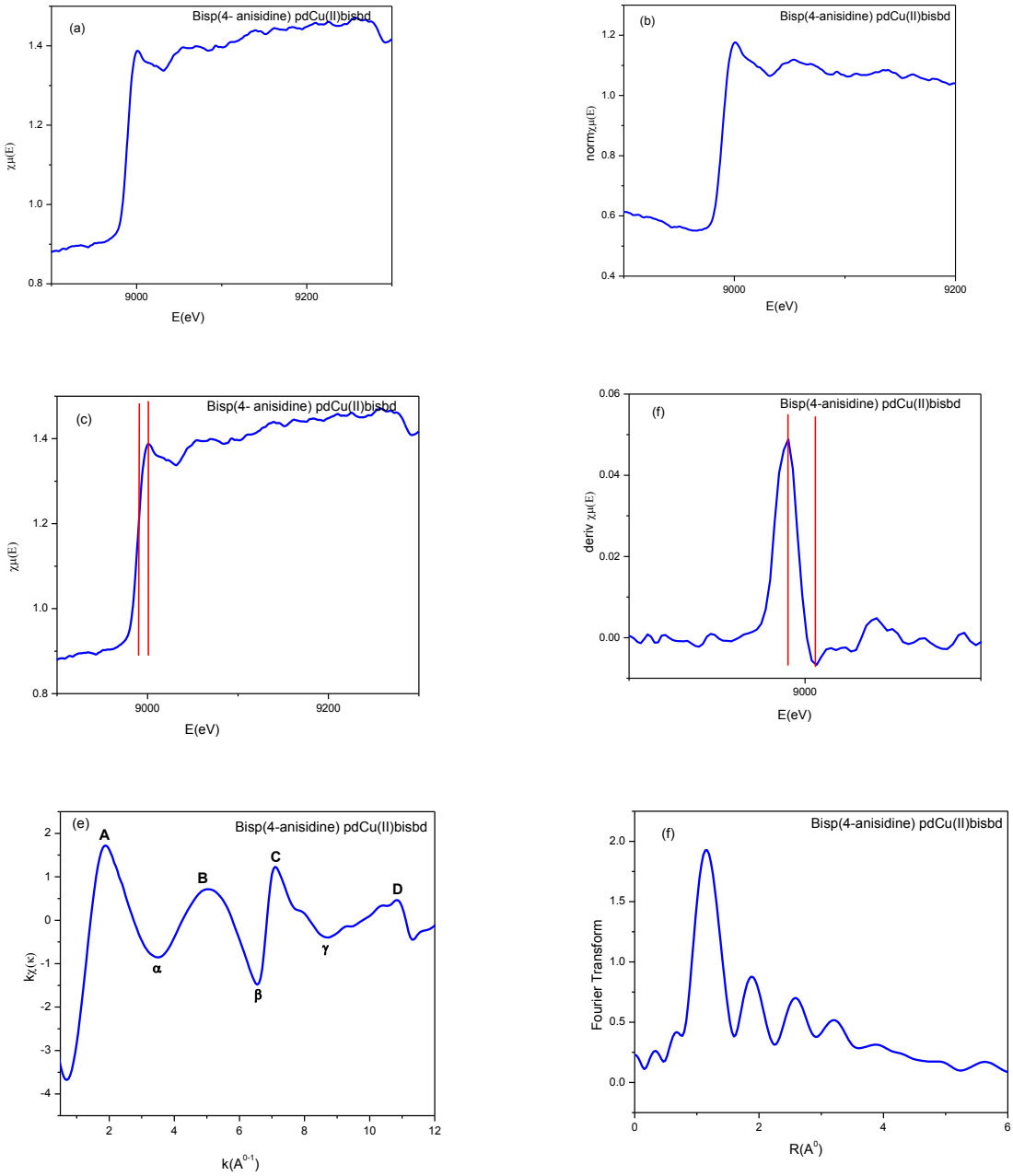

Figure 5-10 XAFS data analysis curves for Bisp(4-anisidine) pdCu(II)bisbd.

(a) Raw absorption versus photoelectron energy (b) The normalized absorption spectrum (c) XAFS spectrum and (d) Derivative of XAFS spectrum for copper metal indicating position of absorption edge K and principal absorption maxima A. (e) χ(k) versus k curve and (f) Magnitude of Fourier transform of the χ(k) versus k curve.

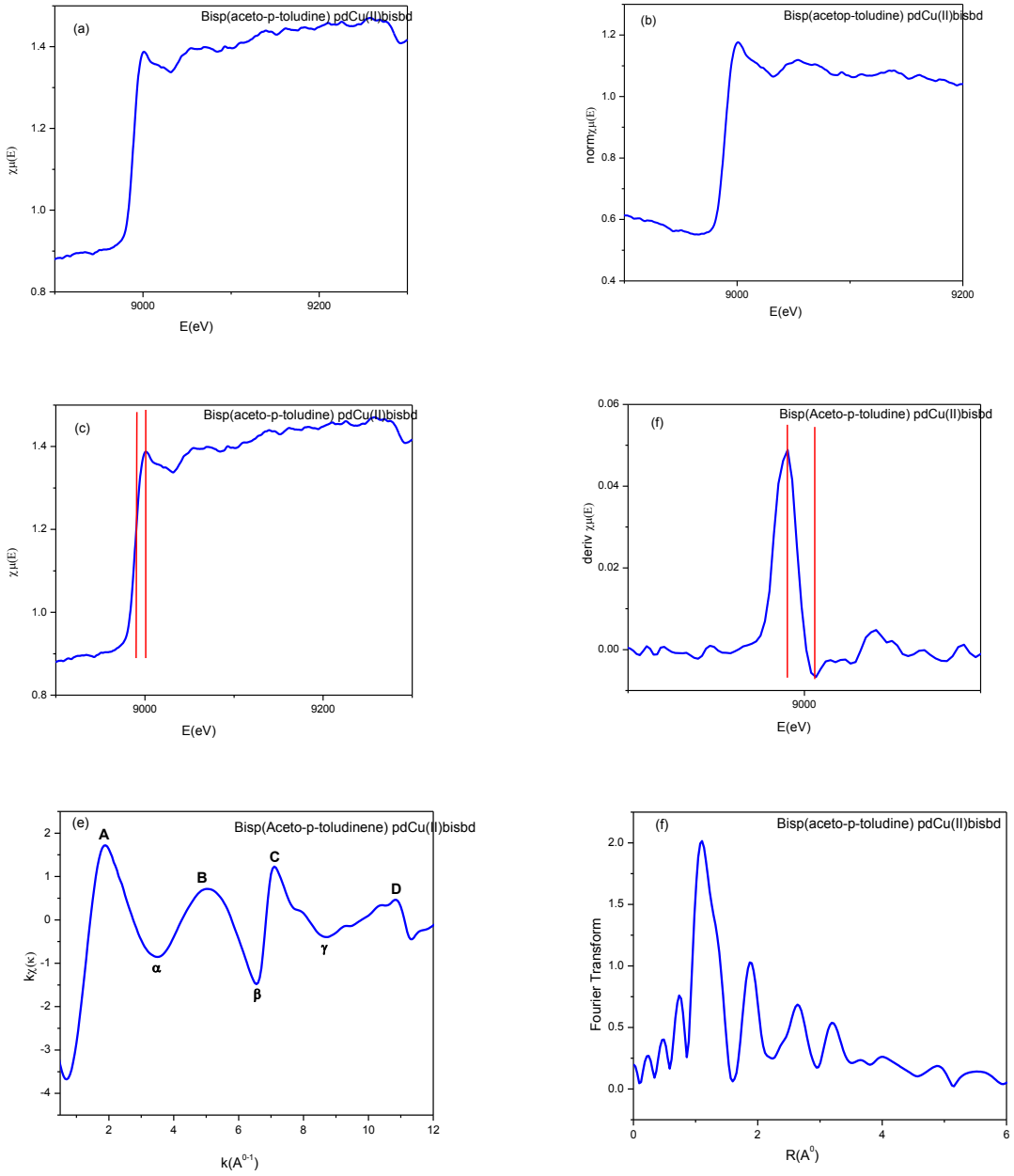

Figure 5-11 XAFS data analysis curves for Bisp(Aceto-p-toludine) pdCu(II)bisbd.

(a) Raw absorption versus photoelectron energy (b) The normalized absorption spectrum (c) XAFS spectrum and (d) Derivative of XAFS spectrum for copper metal indicating position of absorption edge K and principal absorption maxima A. (e) χ(k) versus k curve and (f) Magnitude of Fourier transform of the χ(k) versus k curve.

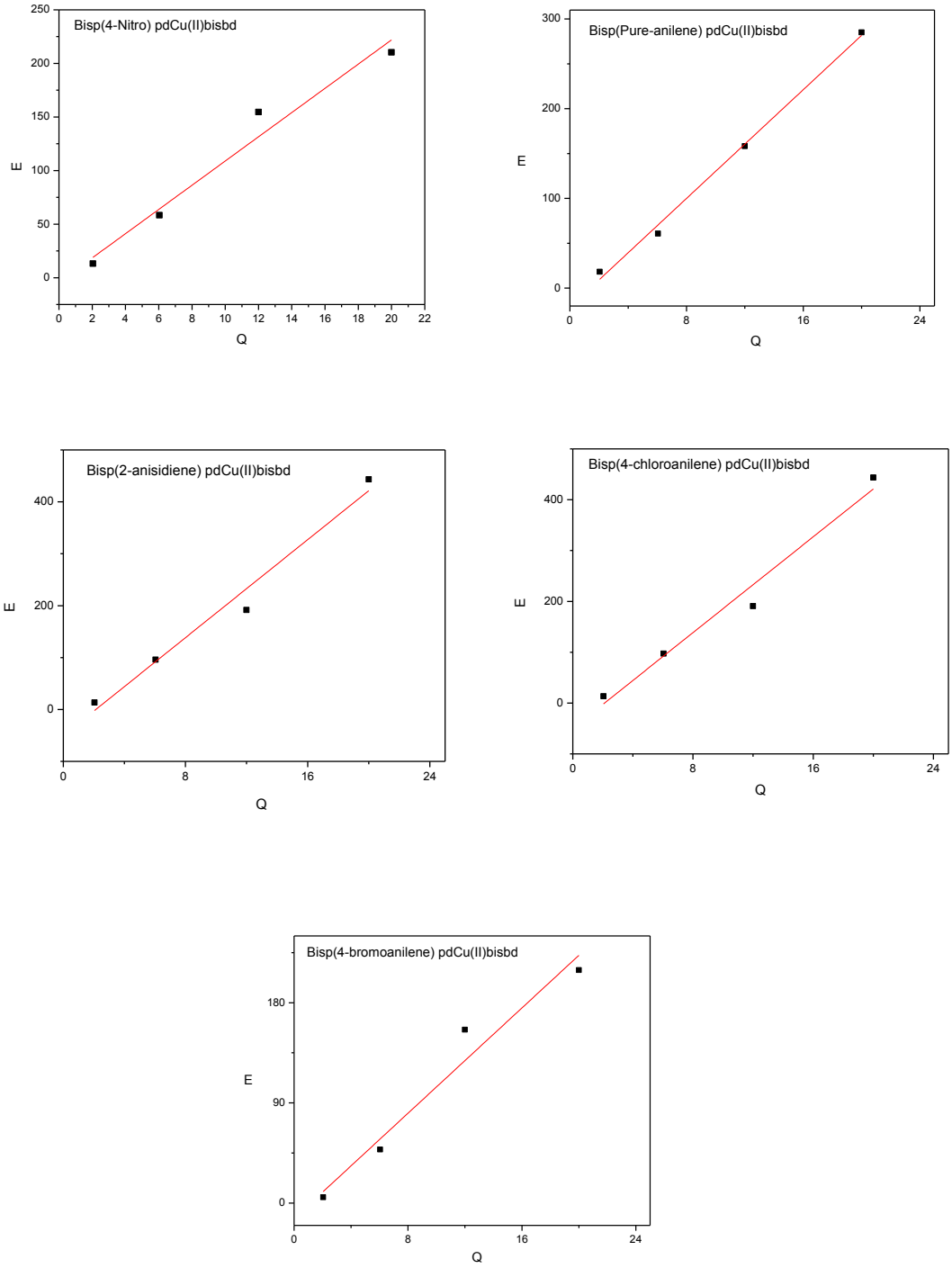

Fig 5-12 E vs. Q curves for Copper (II) complexes.

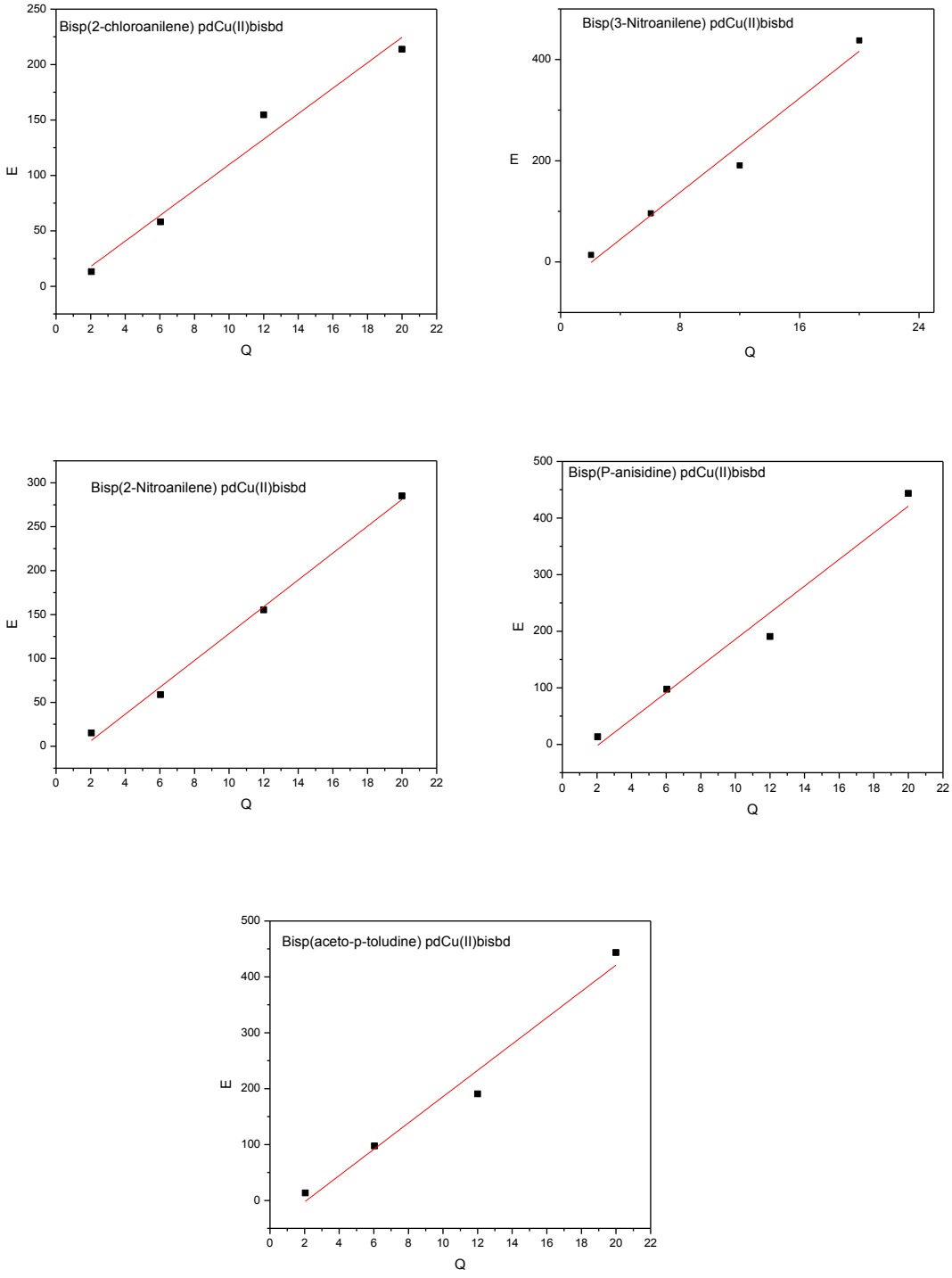

Figure 5-12 E vs. Q curves for Copper (II) complexes.

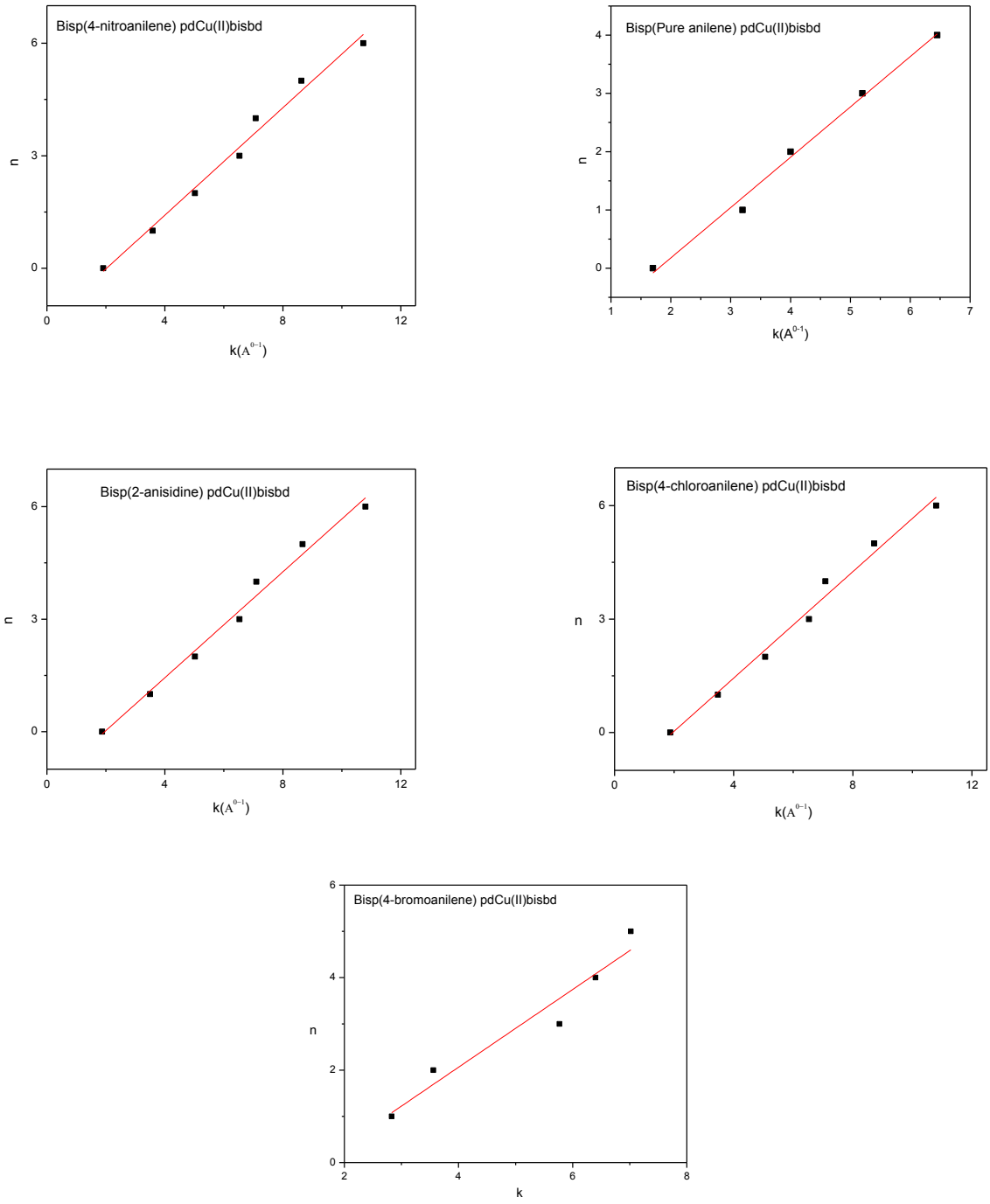

Fig. 5-13 n versus k curves for the copper complexes.

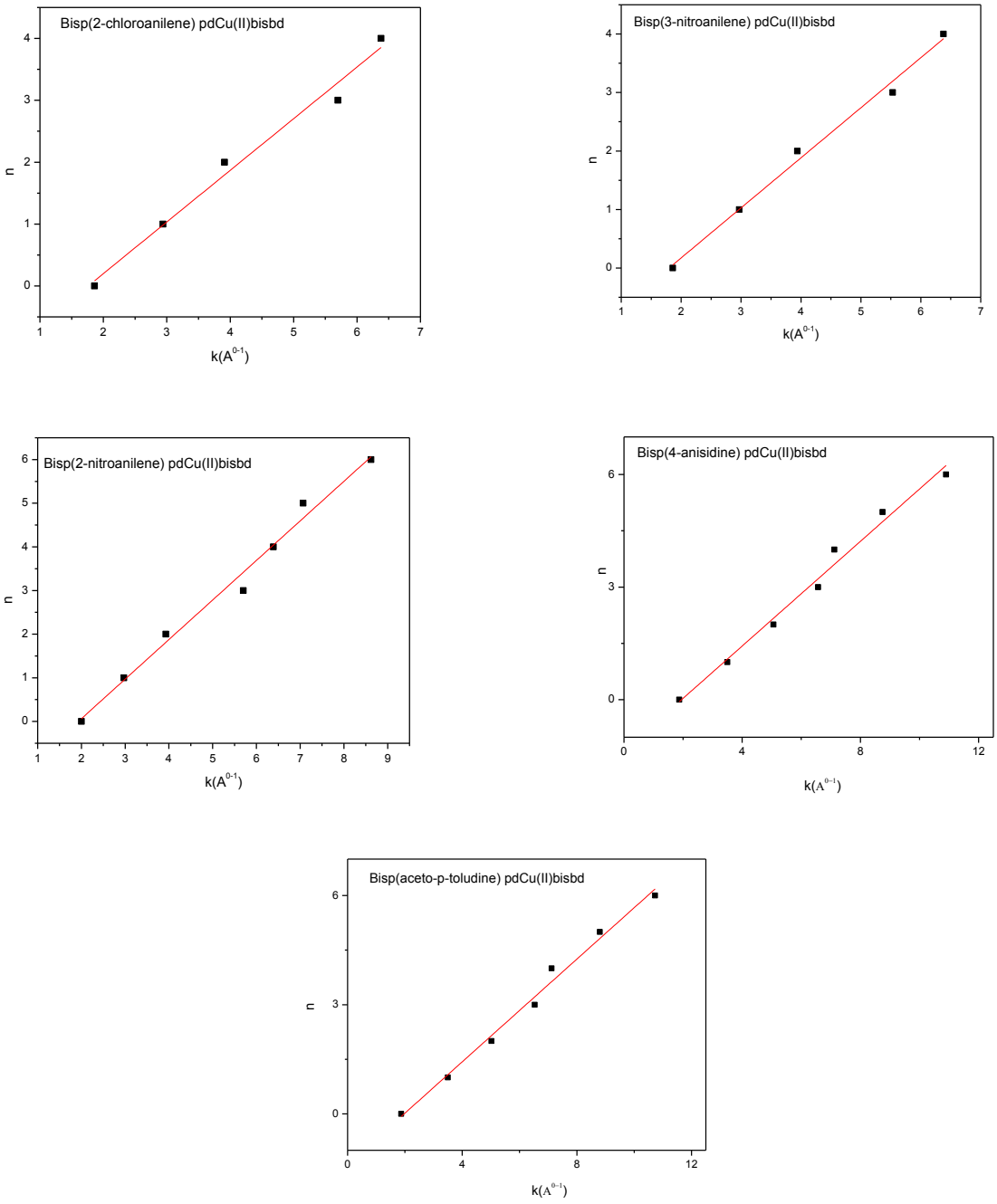

Figure 5-13 n versus k curves for the copper complexes.

***